

Ankyrin-B metabolic syndrome combines age-dependent adiposity with pancreatic β cell insufficiency

Damaris N. Lorenzo,^{1,2} Jane A. Healy,² Janell Hostettler,^{1,2} Jonathan Davis,^{1,2} Jiayu Yang,² Chao Wang,^{3,4} Hans Ewald Hohmeier,^{5,6} Mingjie Zhang,^{3,4} and Vann Bennett^{1,2}

¹Howard Hughes Medical Institute and ²Department of Biochemistry, Duke University, Durham, North Carolina, USA. ³Division of Life Science, State Key Laboratory of Molecular Neuroscience, Hong Kong University of Science and Technology, Hong Kong, China. ⁴Center of Systems Biology and Human Health, School of Science and Institute for Advanced Study, Hong Kong, China. ⁵Department of Medicine and ⁶Sarah W. Stedman Nutrition and Metabolism Center, Duke University, Durham, North Carolina, USA.

Rare functional variants of ankyrin-B have been implicated in human disease, including hereditary cardiac arrhythmia and type 2 diabetes (T2D). Here, we developed murine models to evaluate the metabolic consequences of these alterations in vivo. Specifically, we generated knockin mice that express either the human ankyrin-B variant R1788W, which is present in 0.3% of North Americans of mixed European descent and is associated with T2D, or L1622I, which is present in 7.5% of African Americans. Young *Ankb*^{R1788W/R1788W} mice displayed primary pancreatic β cell insufficiency that was characterized by reduced insulin secretion in response to muscarinic agonists, combined with increased peripheral glucose uptake and concomitantly increased plasma membrane localization of glucose transporter 4 (GLUT4) in skeletal muscle and adipocytes. In contrast, older *Ankb*^{R1788W/R1788W} and *Ankb*^{L1622I/L1622I} mice developed increased adiposity, a phenotype that was reproduced in cultured adipocytes, and insulin resistance. GLUT4 trafficking was altered in animals expressing mutant forms of ankyrin-B, and we propose that increased cell surface expression of GLUT4 in skeletal muscle and fatty tissue of *Ankb*^{R1788W/R1788W} mice leads to the observed age-dependent adiposity. Together, our data suggest that ankyrin-B deficiency results in a metabolic syndrome that combines primary pancreatic β cell insufficiency with peripheral insulin resistance and is directly relevant to the nearly one million North Americans bearing the R1788W ankyrin-B variant.

Introduction

The incidence of obesity, type 2 diabetes (T2D), and related comorbidities has markedly increased during the last 20 years (1, 2). Individual susceptibility to T2D and obesity reflects a complex mix of genetic, epigenetic, and environmental influences that are exacerbated by poor dietary habits and sedentary lifestyles (3). Initial efforts to uncover obesity and T2D susceptibility loci through GWAS have identified common genetic variants with low effect sizes (4, 5), which collectively account for only 10% of disease heritability (6, 7). Moreover, disease variants associated with particular ethnic groups are often undetected in GWAS because these populations are either not included or are underrepresented (8). Increasing evidence suggests that gene variants with frequencies below the GWAS threshold of detection of 5% are also important contributors to complex disease susceptibility (9, 10). The growing availability of whole-exome

and whole-genome sequence information for large numbers of individuals is facilitating the detection of lower-frequency variants that may be associated with common metabolic diseases. However, identifying the variants among these candidates that exhibit a physiological phenotype remains a challenge.

Ankyrin-B (AnkB) is a member of the ankyrin family of membrane adaptors that contributes to the assembly of diverse specialized plasma membrane domains (11). In addition, AnkB associates with phosphatidylinositol 3-phosphate in intracellular membranes and with the dynactin/dynein motor complex to facilitate microtubule-based organelle transport (12–14). In the heart, AnkB regulates Ca²⁺ dynamics through localization of the sodium pump, the sodium/calcium exchanger, and inositol-1, 4, 5-trisphosphate receptors (InsP3Rs) to transverse tubules of cardiomyocytes (15, 16). Nonsynonymous mutations in *ANKB* have been linked to a hereditary cardiac arrhythmia syndrome and are present at frequencies from 0.05% to 7% in human populations, depending on ethnicity (refs. 15–18 and Figure 1A).

AnkB is enriched in pancreatic β cells, where it stabilizes InsP3R and regulates intracellular Ca²⁺ release, functions required for enhanced insulin secretion in response to muscarinic agonists (19). AnkB-haploinsufficient (*Ankb*^{+/-}) mice exhibited impaired oral glucose tolerance, with reduced cholinergic potentiation of glucose-stimulated insulin secretion. Interestingly, the cardiac arrhythmia-associated human p.R1788W AnkB variant is enriched in probands of mixed European descent and Hispanic probands

Note regarding evaluation of this manuscript: Manuscripts authored by scientists associated with Duke University, The University of North Carolina at Chapel Hill, Duke-NUS, and the Sanford-Burnham Medical Research Institute are handled not by members of the editorial board but rather by the science editors, who consult with selected external editors and reviewers.

Conflict of interest: The authors have declared that no conflict of interest exists.

Submitted: February 3, 2015; **Accepted:** May 27, 2015.

Reference information: *J Clin Invest*. 2015;125(8):3087–3102. doi:10.1172/JCI81317.

with T2D from the American Diabetes Association GENNID cohort, relative to its rare incidence in control groups as well as in other ethnically matched populations (Figure 1B and refs. 19–21). In comparison to wild-type AnkB, expression of the R1788W AnkB variant failed to rescue insulin secretion deficits in AnkB-deficient pancreatic islets, suggesting that this variant is likely to cause defective glycemic regulation through impaired AnkB function and is a risk factor for T2D and associated disorders (19).

To evaluate the physiological consequences of human AnkB variants, we generated knockin mice bearing the p.R1788W mutation, linked to T2D, and the p.L1622I variant, the most common ANKB mutation in African Americans at over 7%, with a presence in less than 0.1% of individuals of mixed European descent (Figure 1A and refs. 17–20). The p.L1622I AnkB variant, characterized in the setting of hereditary cardiac arrhythmia, has demonstrated functional effects in cardiomyocytes (17, 18). Although this variant did not associate with T2D in the GENNID cohort, within this group it was exclusively identified in patients of African American descent, who are known to have a greater risk of diabetes than counterparts of mixed European descent. We hypothesized that p.L1622I AnkB might promote more subtle metabolic derangements that, in combination with other genetic, environmental, and lifestyle factors, could promote diabetogenesis. Here, we show that mice homozygous for either the R1788W or L1622I alterations develop a metabolic syndrome characterized by early-onset pancreatic β cell dysfunction and age- or diet-dependent increased adiposity and insulin resistance. We explore the mechanistic basis for these phenotypes, determining that these AnkB variants influence insulin secretion in pancreatic β cells acting through InsP3Rs. Furthermore, we demonstrate for the first time to our knowledge that AnkB promotes internalization of GLUT4 from the plasma membrane and present evidence that increased cell surface GLUT4 in *Ankb*^{R1788W/R1788W} mice results in age-dependent adiposity and insulin resistance.

Results

Human AnkB variants cause tissue-specific AnkB deficiency. We generated knockin mice bearing either the T2D-associated R1788W variant or the L1622I variant (Supplemental Figure 1A; supplemental material available online with this article; doi:10.1172/JCI81317DS1). R1788 and L1622 residues are located in the unstructured C-terminal regulatory domain of AnkB and are conserved from humans to chickens (Figure 1, C and D, and ref. 22). The R1788W and L1622I variants were predicted to be damaging by computational structural modeling, including the Polyphen-2 algorithm (R1788W score = 1 and L1622I score = 0.975). R1788W was also expected to be damaging by sorting intolerant from tolerant (SIFT) analysis (score = 0.001). We found that functional changes could not be attributed to effects of these human variants on AnkB secondary or tertiary structure, as recombinant AnkB polypeptides containing the R1788W and L1622I substitutions had no effect on AnkB's secondary structure in assays of circular dichroism spectroscopy and chymotryptic digestion (Supplemental Figure 1, B and C).

L1622I and R1788W AnkB variants are predominantly found in heterozygous carriers in human populations. However, to facilitate the detection of early metabolic deficits, we initially characterized

phenotypes of homozygous R1788W (*Ankb*^{R1788W/R1788W}) and L1622 (*Ankb*^{L1622I/L1622I}) AnkB knockin mice. Congenic *Ankb*^{R1788W/R1788W} and L1622 *Ankb*^{L1622I/L1622I} mice, confirmed by DNA sequence analysis, were born at the expected Mendelian ratios and exhibited no differences in *Ankb* mRNA levels, as assessed by quantitative PCR (qPCR) analysis (Figure 1, E and G). To investigate the functional impact of these AnkB variants in vivo, we first evaluated their effect on protein levels. Surprisingly, given the evidence for normal protein folding and unaltered mRNA levels, mice homozygous for AnkB variants R1788W and L1622I had significant reductions in AnkB protein levels in a subset of tissues, including fat, liver, skeletal muscle, pancreatic β cells, and heart. By comparison, no change in AnkB protein expression was detected in brain (Figure 1F and Supplemental Figure 1D). In addition, primary mouse embryonic fibroblast (MEF) cultures derived from *Ankb*^{R1788W/R1788W} and *Ankb*^{L1622I/L1622I} mice showed reduced AnkB protein expression (Figure 1F and Supplemental Figure 1D).

Analysis of protein turnover in cycloheximide-treated MEFs revealed that, in control cells, AnkB expression was reduced to 55% 4 hours after blocking protein synthesis (Supplemental Figure 2, A and B). In contrast, AnkB levels were already reduced to 36% and 47% in untreated *Ankb*^{R1788W/R1788W} and *Ankb*^{L1622I/L1622I} MEFs, respectively, and were unaffected by cycloheximide treatment (Supplemental Figure 2, A and B). These data suggested that these AnkB variants specifically affect the stability of a rapidly degradable AnkB subpopulation. To determine what cellular pathways accounted for the observed decrease in AnkB expression in *Ankb*^{L1622I/L1622I} and *Ankb*^{R1788W/R1788W} mice, we treated MEFs with inhibitors of various protein degradation systems. Our results indicate that calpain, lysosomal, and proteasomal pathways cleared the mutant AnkB polypeptides at higher rates than the control AnkB protein and were partially responsible for their lower levels (Supplemental Figure 2C).

R1788W AnkB mutation impairs insulin secretion and oral glucose tolerance. Deficits in AnkB and InsP3R levels noted in *Ankb*^{+/-} mice (19) were recapitulated in islets of 3-month-old *Ankb*^{R1788W/R1788W} and *Ankb*^{L1622I/L1622I} mice (Figure 1F, Figure 2A, and Supplemental Figure 1D). Similar to those of *Ankb*^{+/-} mice, isolated pancreatic islets of *Ankb*^{R1788W/R1788W} mice exhibited over 50% reduction in glucose-stimulated insulin secretion normalized to total insulin content. By contrast, islets isolated from *Ankb*^{L1622I/L1622I} mice responded normally to glucose stimulation (Figure 2B).

While fasting serum glucose levels were unaltered in both *Ankb*^{R1788W/R1788W} and *Ankb*^{L1622I/L1622I} mice, oral administration of glucose (2 g/kg body weight) during an oral glucose tolerance test led to both an increased level of blood glucose at 30 minutes as well as a delay in glucose clearance (Figure 2D and Supplemental Figure 3A). The areas under the curve for the blood glucose response were significantly increased by 2- and 1.7-fold in *Ankb*^{R1788W/R1788W} and *Ankb*^{L1622I/L1622I} knockin mice, respectively (Figure 2E), and by 1.8- and 1.4-fold in heterozygous carriers of the same genotypes, designated as *Ankb*^{R1788W/+} and *Ankb*^{L1622I/+} mice (Supplemental Figure 3B), when compared with control littermates. Consistent with impaired glucose clearance, *Ankb*^{R1788W/R1788W} mice exhibited 50% reduction in serum insulin levels following glucose ingestion (Figure 2C). In contrast, both *Ankb*^{R1788W/R1788W} and *Ankb*^{L1622I/L1622I} mice displayed normal tolerance to glucose administered through intra-

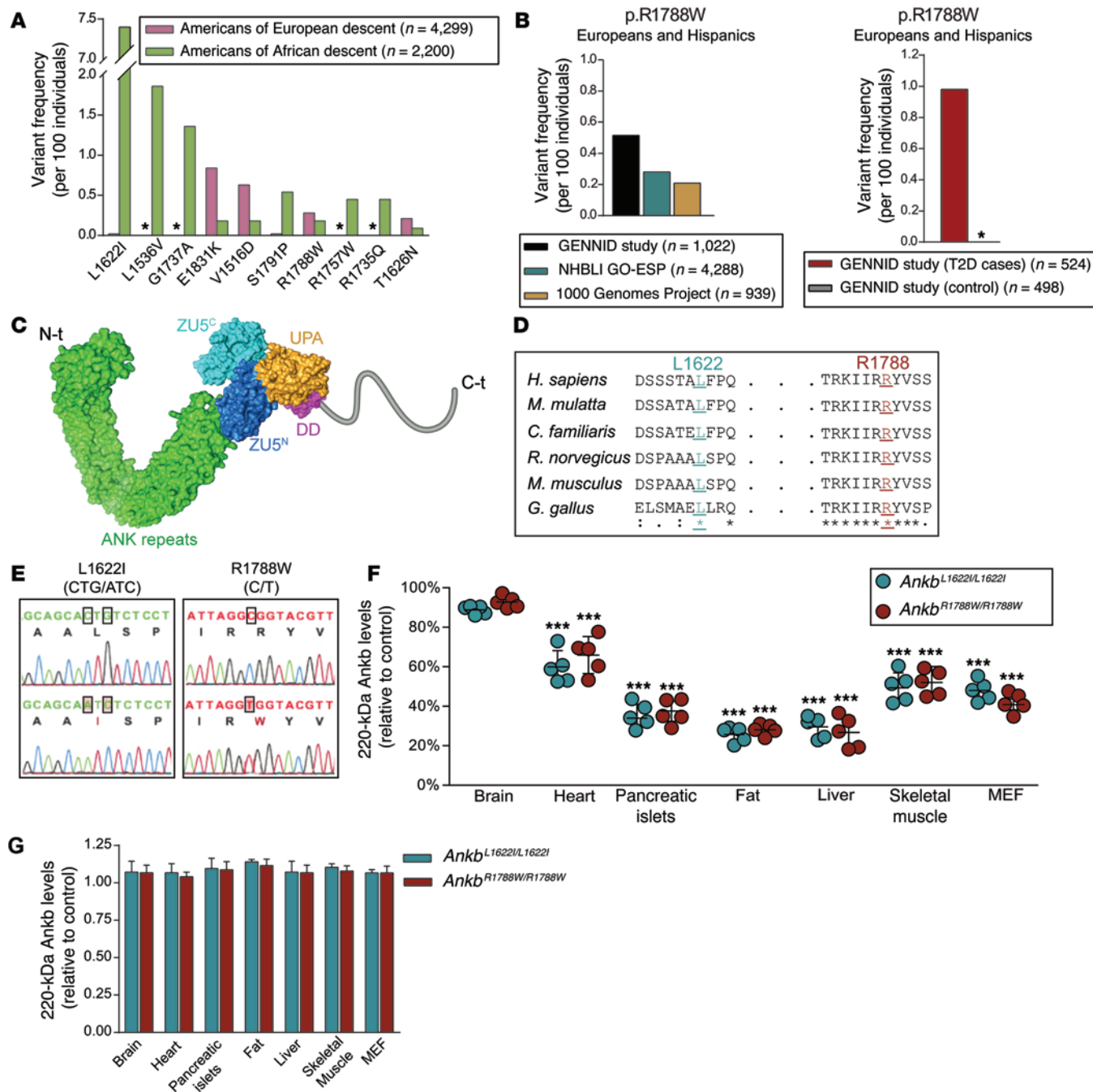


Figure 1. Human AnkB variants cause tissue-specific AnkB reduction. (A) Variant frequency (per 100 individuals) for the most common *ANKB* variants in North Americans of European and African descent. Allele frequencies were compiled from the NHLBI GO Exome Sequencing Project. Asterisks indicate undetected variants. (B) Frequency of the p.R1788W *ANKB* variant in European Americans and Hispanics from the GENNID cohort of noninsulin-dependent diabetic patients (control and T2D cases) and from individuals of the same ethnicity sequenced as part of the entire GENNID cohort, the NHLBI GO Exome Sequencing Project, and the 1000 Genomes Project. Asterisks indicate undetected variants. (C) Model of AnkB structure, with domains indicated, showing the localization of L1622 and R1788 sites within AnkB's unstructured C-terminal domain. (D) Evolutionary conservation of L1622 and R1788 sites. (E) Sequencing chromatograms of brain cDNA from *Ankb*^{+/+} and *Ankb* knockin mice. (F) Quantitative analysis of AnkB protein levels for the indicated tissues as a percentage of control (*Ankb*^{+/+}). (G) Quantification of 220-kDa *Ankb* transcript levels by qPCR. GAPDH was used for normalization of mRNA and protein levels. Data represent mean \pm SEM ($n = 5$ males, 10-weeks-old). Results are representative of 3 independent experiments. *** $P < 0.001$, 2-tailed t test.

peritoneal injection relative to that of *Ankb*^{+/+} controls (Supplemental Figure 4). The finding of normal intraperitoneal glucose tolerance but impaired oral glucose tolerance was also reported for *Ankb*^{+/-} mice and was rationalized to be due to loss of cholinergic enhancement of insulin secretion, which occurs following oral intake of glucose (19).

In pancreatic β cells, InsP3R regulates Ca²⁺ mobilization and cholinergic potentiation of glucose-stimulated insulin secretion. InsP3R deficiency results in hyperglycemia and glucose intolerance in young mice (23–25), without affecting insulin sensitivity (Supplemental Figure 5). Interestingly, 3-month-old InsP3R-haploinsufficient (*Itpr1*^{+/-}) mice exhibited abnormal oral glucose tolerance and insulin secretion deficits following oral glucose ingestion, which were similar to the phenotypes observed in young *Ankb*^{R1788W/R1788W} mice (Figure 2, F–H, and ref. 25). However, *Ankb*^{L1622I/L1622I} mice, which also exhibit a reduction in InsP3R, had normal glucose-dependent insulin secretion from isolated islets and normal serum insulin levels following glucose ingestion (Figure 2, B and C). Thus, InsP3R downregulation likely contributes to primary β cell insufficiency in young R1788W mice, while L1622I mice apparently employ additional compensatory mechanism(s).

Increased peripheral glucose uptake in young *Ankb*^{R1788W/R1788W} mice. Despite impaired insulin secretion and abnormal oral glucose tolerance, 3-month-old *Ankb*^{R1788W/R1788W} mice exhibited normal fasting glucose levels (Figure 2E, time 0, and Figure 3A, time 0). To evaluate whole-body glucose utilization, hyperinsulinemic-euglycemic clamp, combined with measurements of 2-deoxy-[³H]-glucose (2-DG) transport in vivo in skeletal muscle and white adipose tissue (WAT), was conducted at the Yale Metabolic Core Facility. Blood glucose levels were tightly maintained through a variable glucose infusion rate (GIR) in response to a constant exogenous supply of insulin. Surprisingly, clamp measurements revealed that 3-month-old *Ankb*^{R1788W/R1788W} mice have increased glucose utilization compared with that of control littermates and *Ankb*^{L1622I/L1622I} mice, as demonstrated by a significantly higher whole-body GIR (Figure 3, A and B). Moreover, 2-DG uptake by *Ankb*^{R1788W/R1788W} mice was significantly elevated compared with that of controls in both skeletal muscles (30%) and WAT (76%) (Figure 3, C and D). By comparison, *Ankb*^{L1622I/L1622I} mice exhibited normal 2-DG uptake in skeletal muscle and a more modest 43% increase in WAT (Figure 3, C and D). In contrast, both *Ankb*^{R1788W/R1788W} and *Ankb*^{L1622I/L1622I} 3-month-old mice showed similar increases in hepatic-insulin responsiveness, as reflected by a 93% suppression of hepatic endogenous glucose production (EGP) during the clamp in *Ankb*^{R1788W/R1788W} mice and a 88% suppression in *Ankb*^{L1622I/L1622I} mice, compared with a 53% suppression in control mice (Supplemental Figure 6, A and B). Changes in EGP were concomitant with reductions in transcript levels for gluconeogenesis rate-limiting enzymes (Supplemental Figure 6E). Together, our results suggest that reduced gluconeogenesis rates contribute to the maintenance of normoglycemia in young *Ankb*^{R1788W/R1788W} and *Ankb*^{L1622I/L1622I} mice. It is notable that suppression of EGP was seen in both *Ankb*^{R1788W/R1788W} and *Ankb*^{L1622I/L1622I} animals, though higher whole-body glucose disposal was observed exclusively in *Ankb*^{R1788W/R1788W} mice. This suggests that increased peripheral glucose uptake, rather than decreased gluconeogenesis, is the primary cause of the accelerated glucose disposal rate detected in the *Ankb*^{R1788W/R1788W} mice.

Blood glucose uptake by skeletal muscle and adipocytes is achieved by glucose transporter 4 (GLUT4), which rapidly translocates to the cell surface from intracellular storage sites in response to insulin (26). Numerous studies suggest that activation of the serine/threonine phosphoinositide 3-kinase and phosphorylation of its downstream target PKB (also known as AKT) are key steps in the regulation of insulin-induced exocytosis of GLUT4-containing vesicles (27–29). Significantly, levels of phosphorylated S473 AKT were similar in skeletal muscle or in differentiated adipocytes across genotypes, both under basal and insulin-stimulated conditions (Figure 3, E and F). These observations suggest that the increased glucose uptake in peripheral tissues of *Ankb*^{R1788W/R1788W} mice is not likely due to global alterations in AKT-dependent activation of insulin signaling. However, we cannot rule out effects of AnkB variants on specific AKT isoforms or other components of the AKT insulin-dependent signaling pathway.

Increased cell-surface GLUT4 in tissues of *Ankb* knockin mice. To investigate the mechanism underlying the increased glucose uptake observed in young *Ankb*^{R1788W/R1788W} mice, we examined the levels of GLUT4 in plasma membrane fractions from extracts of skeletal muscle and adipose tissue either under resting conditions or following exogenous insulin stimulation. Untreated control (*Ankb*^{+/+}) mice showed low levels of plasma membrane-associated GLUT4, which increased around 2-fold upon insulin stimulation (Figure 3, G and I). In contrast, under basal conditions, GLUT4 was robustly associated with plasma membranes from *Ankb*^{R1788W/R1788W} mice (over 2-fold higher GLUT4 cell surface levels than in controls) and, to a lesser extent, from *Ankb*^{L1622I/L1622I} mice. GLUT4 maintained its plasma membrane localization after insulin treatment in both homozygous knockin strains (Figure 3, G and H). Total GLUT4 levels were similar in skeletal muscle and fat across all genotypes (Figure 3I). The elevations in surface-associated GLUT4 under basal conditions were also detected in skeletal muscle and adipose tissue membrane fractions from *Ankb*^{+/-} mice (Figure 3, G and H), suggesting that these deficits are, at least in part, due to reduced levels of AnkB polypeptides. The persistent plasma membrane localization of GLUT4 in skeletal muscle and adipose tissue in young *Ankb*^{R1788W/R1788W} mice provides a potential compensatory mechanism to explain how these animals maintain normal fasting glucose levels in the face of impaired insulin secretion.

AnkB regulates GLUT4 internalization in differentiated adipocytes. To elucidate the role of AnkB in GLUT4 cellular localization, we first assessed glucose uptake in differentiated adipocyte cultures established from primary MEF lines derived from *Ankb*^{+/+}, *Ankb*^{+/-}, *Ankb*^{L1622I/L1622I}, and *Ankb*^{R1788W/R1788W} mice. Similar to the in vivo results, differentiated adipocytes from *Ankb*^{+/-}, *Ankb*^{L1622I/L1622I}, and *Ankb*^{R1788W/R1788W} animals exhibited elevated glucose uptake under both resting conditions and following insulin stimulation (Figure 4A). Next, we assessed the cell surface expression of GLUT4 in adipocytes by transfection with a construct encoding GLUT4-GFP containing an exofacial Myc epitope (Figure 4C). The expressed fusion protein has been shown previously to be fully active in vivo (30). At steady-state, the majority of GLUT4 molecules were intracellular in *Ankb*^{+/+} adipocytes, as measured by the ratio of plasma membrane to cytosolic myc-GLUT4 signal (0.2, Figure 4, D and E, basal). However, cell surface GLUT4 localization increased 3.8-fold following insulin

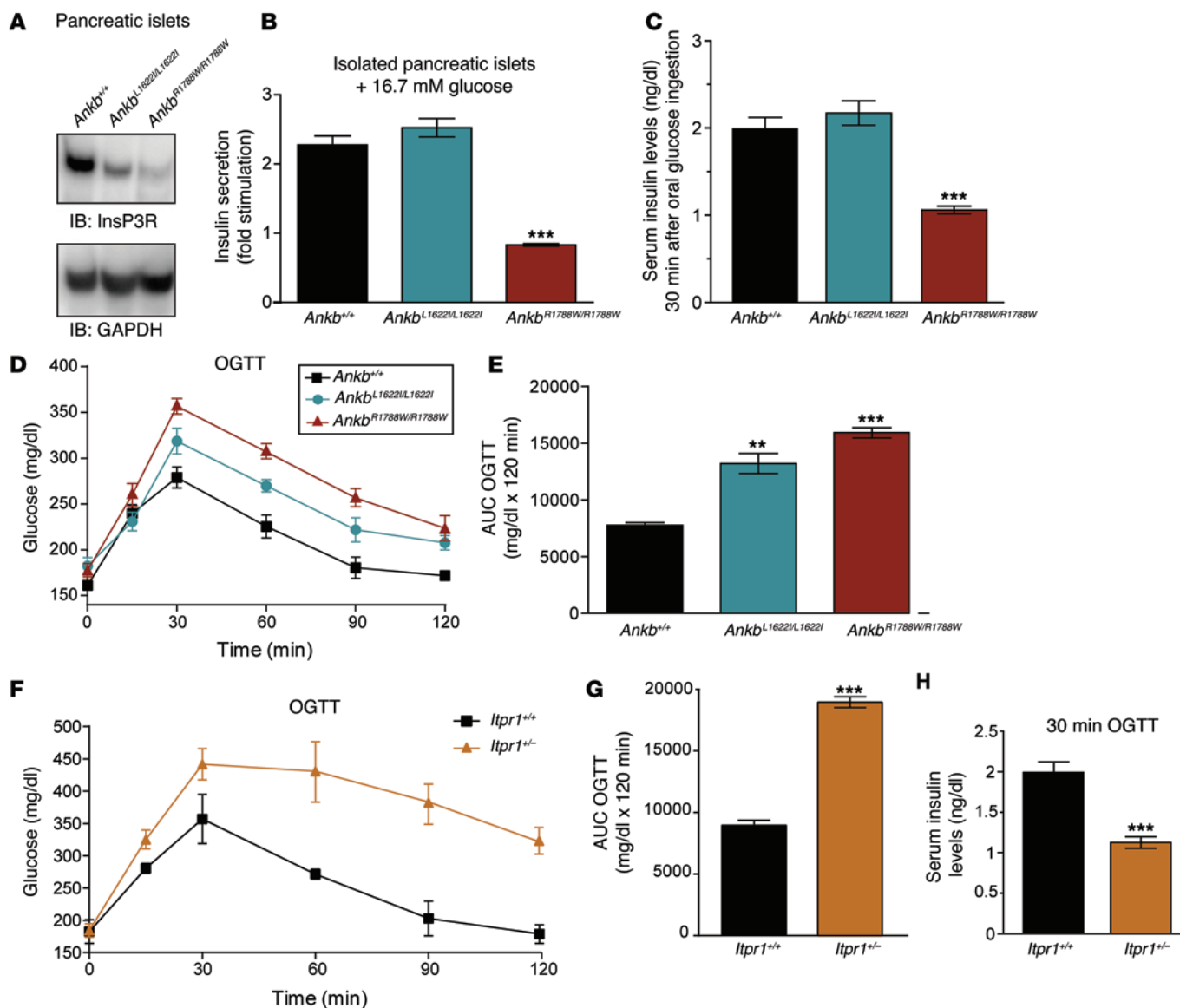


Figure 2. Pancreatic β cell insufficiency secondary to loss of InsP3R, impaired oral glucose tolerance, and insulin secretion deficits in 3-month-old *Ankb*^{R1788W/R1788W} mice. (A) InsP3R and GAPDH protein levels in isolated pancreatic islets of 3-month-old mice. (B) Insulin secretion by cultured pancreatic islets in response to glucose. Data represent mean \pm SEM ($n = 7$ mice, *** $P < 0.001$, 1-way ANOVA with post-hoc Tukey test). (C) Serum insulin levels in *Ankb*^{+/+}, *Ankb*^{L1622I/L1622I}, and *Ankb*^{R1788W/R1788W} mice 30 minutes after oral glucose administration during an oral glucose tolerance test (OGTT). (D) Blood glucose levels in response to oral glucose (2 mg/kg body weight) for the indicated genotypes. (E) Area under the curve for the OGTT. (F) Blood glucose levels in response to oral glucose (2 mg/kg body weight) for 3-month-old control (*Itpr1*^{+/+}) and *Itpr1*^{-/-} mice. (G) Area under the curve for the OGTT. (H) Serum insulin levels 30 minutes after oral glucose administration during an OGTT for control and *Itpr1*^{-/-} mice. Data from C–H represent mean \pm SEM ($n = 10$ mice). ** $P < 0.01$, *** $P < 0.001$, 1-way ANOVA with post-hoc Tukey test. Results are representative of 3 independent experiments.

treatment (Figure 4, D and E, time 0). In contrast, cell surface GLUT4 was already elevated about 2-fold in *Ankb*^{L1622I/L1622I} and 3.2-fold in *Ankb*^{R1788W/R1788W} adipocytes at rest and remained high in the insulin-stimulated state (Figure 4, D and E).

In muscle cells and adipocytes under basal conditions, low levels of GLUT4 on the cell surface are maintained by a faster rate of GLUT4 endocytosis relative to re-exocytosis (31, 32). Considering that we did not observe significant increases in the rate of GLUT4 translocation to the surface in response to insulin in *Ankb*^{R1788W/R1788W} or *Ankb*^{L1622I/L1622I} adipocytes compared with that

in *Ankb*^{+/+} adipocytes (Figure 4D, time 0), we hypothesized that elevation in GLUT4 on the surface of cells isolated from *Ankb* knockin mice resulted from a slower internalization rate. Monitoring of GLUT4 endocytosis in differentiated control adipocytes after insulin stimulation showed markedly increased plasma membrane localization (Figure 4D, time 0) increased plasma membrane localization (Figure 4D, time 0), which decreased to nonstimulated values (Figure 4, D and E) 30 minutes after internalization ($t_{1/2}$ of GLUT4 internalization = 7 minutes). In contrast, plasma membrane-associated Myc-GLUT4-GFP

in *Ankb*^{R1788W/R1788W} adipocytes doubled compared with that in *Ankb*^{+/+} adipocytes at the same time interval and exhibited a substantial reduction in internalization rate ($t_{1/2}$ = 26 minutes) (Figure 4, D and E). Adipocytes from *Ankb*^{L1622I/L1622I} mice showed an intermediate phenotype ($t_{1/2}$ = of 13 minutes) (Figure 4, D and E). Expression of wild-type 220-kDa AnkB-HA in *Ankb*^{R1788W/R1788W} adipocytes rescued the deficits in the cellular distribution and internalization of GLUT4 ($t_{1/2}$ = 8 minutes) (Figure 4, D and E).

AnkB recruits binding partners to specialized membrane domains and associates with PtdIns(3)P-enriched membranes, such as endosomes, to promote organelle transport (11, 14). Interestingly, AnkB directly interacts with members of the Eps15 homology domain/receptor-mediated endocytosis-1 (EHD/RME-1) family of endosome-based scaffolding molecules and with clathrin heavy chain, both of which have well-established roles in the regulation of GLUT4 intracellular traffic (33–37). Therefore, we hypothesized that AnkB, either directly or in combination with its binding partners, might facilitate GLUT4 retrieval from the plasma membrane. To explore this possibility, we first determined whether AnkB and GLUT4 proteins associate in vivo. Coimmunoprecipitation experiments with skeletal muscle homogenates showed that these proteins interact (Figure 4B). Similarly, coimmunoprecipitation of lysates of HEK293 cells expressing 220-kDa AnkB-GFP and HA-GLUT4 showed binding of AnkB to GLUT4. Anti-GFP antibody coimmunoprecipitated wild-type HA-GLUT4 with AnkB-GFP (Figure 4F). However, it failed to pull down HA-tagged GLUT4 harboring the A⁵AAA⁸ substitutions in the N-terminal F⁵QQI⁸ motif (Figure 4F). This alteration has been previously shown to regulate GLUT4 intracellular sequestration by facilitating its interaction with the endocytic machinery located at the cell surface (38–40).

We further characterized the GLUT4-AnkB interaction by isothermal titration calorimetry, using purified peptides corresponding to residues 1–24 of human GLUT4 and to the ANK repeats of AnkB (residues 1–847), both expressed in bacteria (Supplemental Figure 7A). However, we found that the ANK repeat domain of AnkB failed to associate with the N-terminal portion of GLUT4. In contrast, this domain formed a high-affinity interaction with residues 1206–1233 of the mouse L1 cell adhesion molecule (L1CAM), a known ankyrin-binding partner (Supplemental Figure 7, A and B, and ref. 41). Thus, AnkB interaction with GLUT4 is not mediated by direct interaction of the N-terminal GLUT4 residues with the ANK repeat domain. This suggests that the observed coimmunoprecipitation of GLUT4 and AnkB may require the intact GLUT4 polypeptide and/or involve accessory protein(s).

A single substitution of the phenylalanine residue within the F⁵QQI⁸ motif (F⁵A) causes loss of GLUT4 localization to cell surface clathrin lattices, reduction in GLUT4 internalization, and accumulation of GLUT4 on the plasma membrane of nonstimulated adipocytes (40). To further assess whether AnkB facilitates GLUT4 internalization by mediating its interaction with the endocytic components through the FQQI motif, we evaluated the cellular distribution of the F⁵A Myc-GLUT4-GFP mutant protein in *Ankb*^{+/+} and *Ankb*^{R1788W/R1788W} adipocytes. We found that GLUT4 was internalized at similar rates in *Ankb*^{R1788W/R1788W} adipocytes expressing wild-type Myc-GLUT4-GFP ($t_{1/2}$ = 25 minutes) or mutant F5A Myc-GLUT4-GFP ($t_{1/2}$ = 24 minutes) pro-

teins (Figure 4, D and E) as well as in *Ankb*^{+/+} cells expressing the internalization-deficient F⁵A GLUT4 mutant ($t_{1/2}$ = 25 minutes) (Figure 4E). These results indicate that AnkB deficiency does not affect the internalization deficits of mutant F⁵A GLUT4.

Moreover, these findings suggest that AnkB facilitates the association of GLUT4 with endosomes through the FQQI motif, either directly through domains other than the ANK repeats or through intermediate proteins. This suggests that AnkB might function as a heretofore undescribed adaptor for the endocytic machinery that promotes retrieval of the GLUT4 transporter from the cell surface.

Age-dependent increase in adiposity in R1788W AnkB mice. Increased GLUT4 expression in adipose tissue leads to a constitutive elevation in glucose uptake with increased adiposity in mice (42, 43). Similarly, significantly elevated basal glucose uptake and GLUT4 levels occur in adipocytes from young obese Zucker rats when compared with lean littermates (44). We therefore evaluated effects of age on the extent and distribution of adipose tissue in *Ankb*^{+/+}, *Ankb*^{L1622I/L1622I}, and *Ankb*^{R1788W/R1788W} mice. Young (3-month-old) AnkB knockin mice had a percentage of body fat indistinguishable from that of controls (Figure 5B and Figure 6D). However, older (10-month-old) *Ankb*^{R1788W/R1788W} mice exhibited increased body fat mass, as measured by nuclear magnetic resonance (Figure 5B and Figure 6D). In addition, both *Ankb*^{R1788W/R1788W} and *Ankb*^{L1622I/L1622I} mutant mice exhibited significant adipocyte hypertrophy (54% increase in adipocyte diameter in *Ankb*^{R1788W/R1788W} and 38% in *Ankb*^{L1622I/L1622I} mice; Figure 5, A and C), which was accompanied by elevated levels of circulating nonesterified fatty acids (Figure 5D). Interestingly, these increases in body fat were more prominent than the overall changes in total body weight (Figure 6, A–C). These findings, together with the similar percentages of lean mass observed among all genotypes tested (Figure 6E), suggest that expression of these AnkB variants is associated with a redistribution of body mass, favoring the accumulation of adipose tissue. Thus, our results indicate that, while increased glucose clearance may initially compensate for hyperglycemia caused by impaired insulin production, the persistent rise in glucose uptake by insulin target organs triggers age-dependent increases in adiposity in older animals.

Adult-onset obesity is commonly caused by dysfunction of the hypothalamic circuits regulating energy homeostasis (45, 46). Surprisingly, systematic metabolic cage analysis revealed that both 3-month-old and 10-month-old *Ankb*^{R1788W/R1788W} and *Ankb*^{L1622I/L1622I} mice showed overall similar average rates of food intake, energy source utilization, and activity compared with littermate controls during both light and dark cycles (Figure 6, F–M). These results suggest that the increased body weight and adiposity observed in older *Ankb*^{R1788W/R1788W} and *Ankb*^{L1622I/L1622I} mice are not due to marked changes in appetite or activity. However, our data do not exclude small cumulative effects of decreased activity and/or increased food consumption that were below the sensitivity of these assays or other changes in water content, lean mass, and food absorption in the gut.

Cell-autonomous increases in lipid accumulation in AnkB mutant adipocytes. We next asked whether increased adiposity in vivo could be recapitulated in a cell-autonomous manner in adipocytes differ-

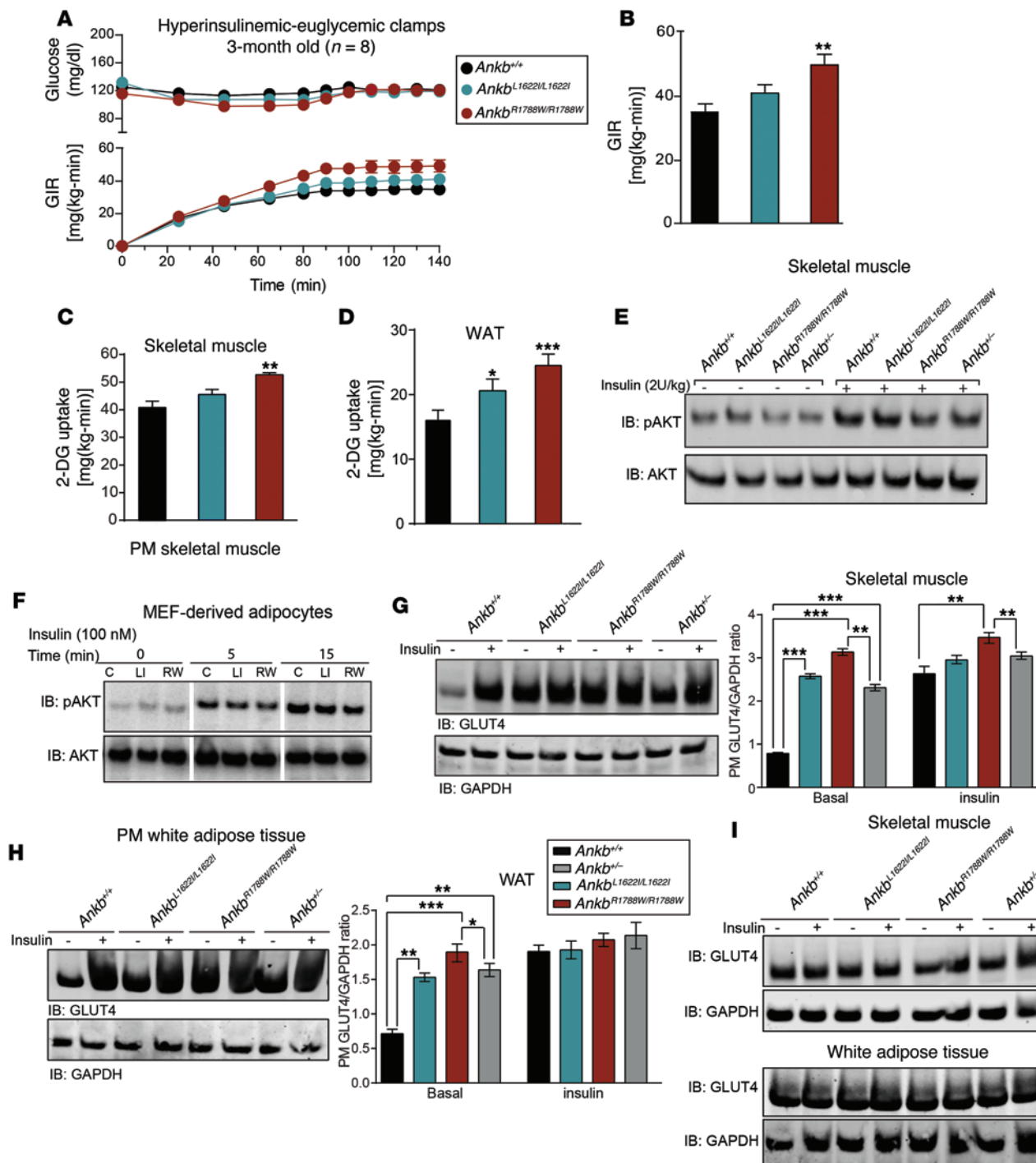


Figure 3. Increased peripheral glucose utilization associated with persistent cell surface GLUT4 in $Ankb^{R1788W/R1788W}$ mice. (A) Hyperinsulinemic-euglycemic clamp analysis in 3-month-old ($n = 8$) mice. (B) GIR during insulin clamp. (C and D) 2-DG uptake by (C) skeletal muscle and (D) WAT. (E and F) Immunoblots of total AKT and phosphorylated AKT (p-AKT S473) levels in (E) skeletal muscle and (F) differentiated adipocytes from 3-month-old mice under basal or insulin-stimulated conditions. (G and H) Immunoblots and quantification of plasma membrane-associated GLUT4 levels after subcellular fractionation of (G) skeletal muscle and (H) WAT lysates under basal conditions or following insulin stimulation. (I) Total levels of GLUT4, as evaluated by immunoblotting. Data represent mean \pm SEM ($n = 8$ mice). * $P < 0.05$, ** $P < 0.01$, *** $P < 0.001$, 1-way ANOVA with post-hoc Tukey test. Results are representative of 3 independent experiments.

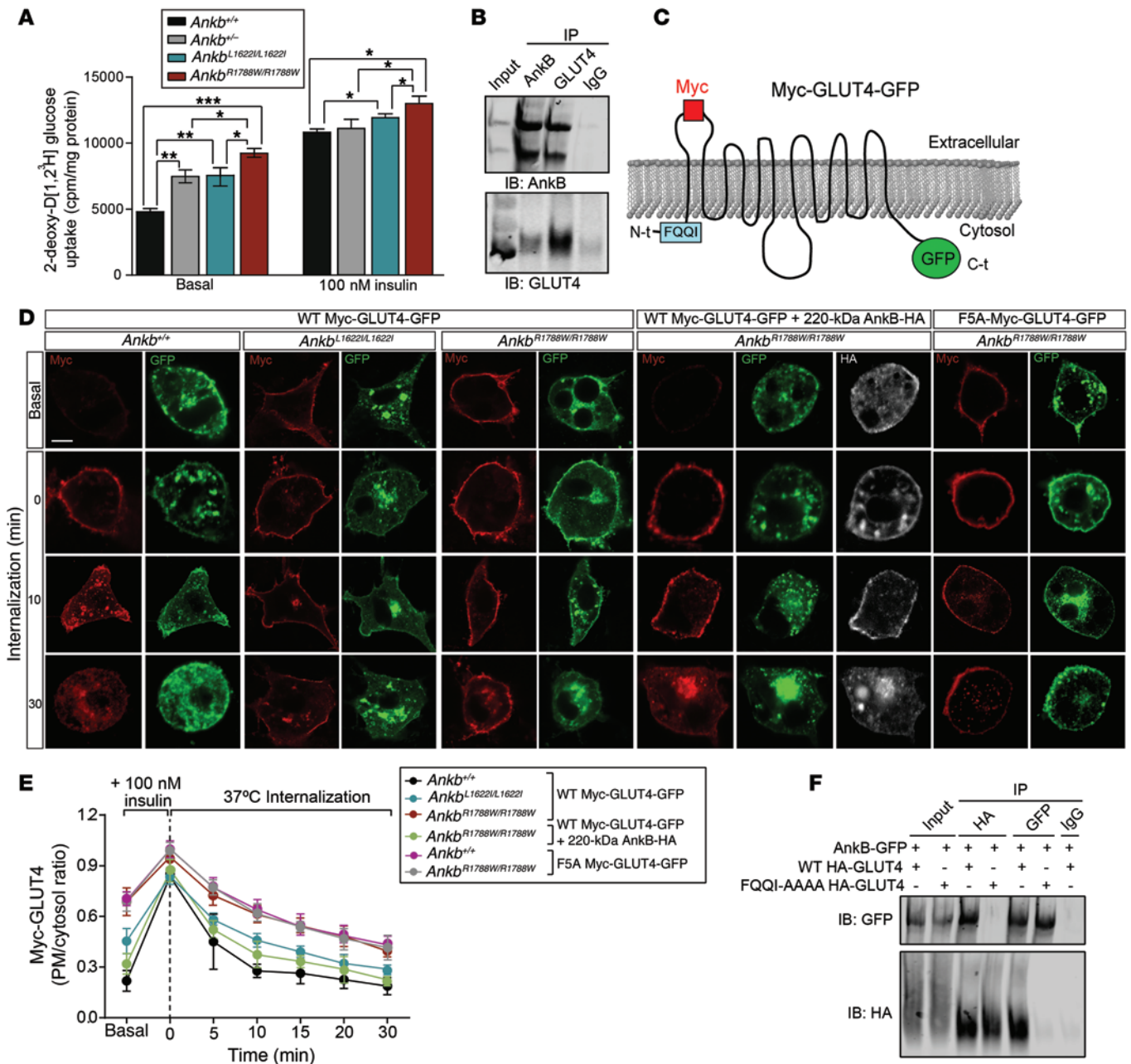


Figure 4. Increased GLUT4 association with plasma membranes of mutant AnkB adipocytes caused by reduced GLUT4 internalization rates. (A) 2-DG uptake in differentiated adipocytes before and after stimulation with 100 nM insulin. Data represent mean \pm SEM of values from one 6-well plate per genotype for 1 of 3 repeats. (B) Coimmunoprecipitation from control mouse skeletal muscle homogenates. (C) Diagram of a GLUT4 construct with extracellular Myc and C-terminal GFP epitopes (Myc-GLUT4-GFP) used for assessing GLUT4 distribution in differentiated adipocytes. The position of the F²QQL motif is indicated. (D) GLUT4 localization in differentiated adipocytes under basal conditions or following insulin stimulation and internalization at 37°C. Scale bar: 10 μ m. (E) Quantification of GLUT4 association with plasma membranes of differentiated adipocytes either at rest or at indicated times following treatment with 100 nM insulin and internalization at 37°C. (F) Coimmunoprecipitation from HEK293 cells expressing either wild-type HA-GLUT4 or F²QQL⁸-A³AAA⁸ HA-GLUT4 and GFP-AnkB proteins. Data is representative of 3 independent experiments. Data represent mean \pm SEM for 1 of 3 independent determinations ($n = 30$ cells per genotype and per condition). * $P < 0.05$, ** $P < 0.01$, *** $P < 0.001$, 1-way ANOVA with post-hoc Tukey test.

entiated from primary MEF cells. Consistent with the phenotype of mice overexpressing GLUT4 in WAT (42) and with our *in vivo* findings (Figure 5, A–C), MEF cultures from *Ankb*^{+/+}, *Ankb*^{L1622I/L1622I}, and *Ankb*^{R1788W/R1788W} mice showed increases in adipogenesis, with both increased numbers of adipocytes and enlarged lipid droplets (Figure 5, E and F, and Supplemental Figure 8A). Importantly, these *in vitro* results suggest that AnkB deficiency can promote adiposity.

The differences in adipocyte differentiation *in vitro* correlated with an earlier and more robust transcriptional activation of genes implicated in adipogenesis (Supplemental Figure 8, B–E). However, similar changes in the expression profile of adipogenesis-related transcription factors and their targets were not observed before the onset of adiposity in adipose tissue of 3-month-old *Ankb*^{R1788W/R1788W} and *Ankb*^{L1622I/L1622I} mice (Supple-

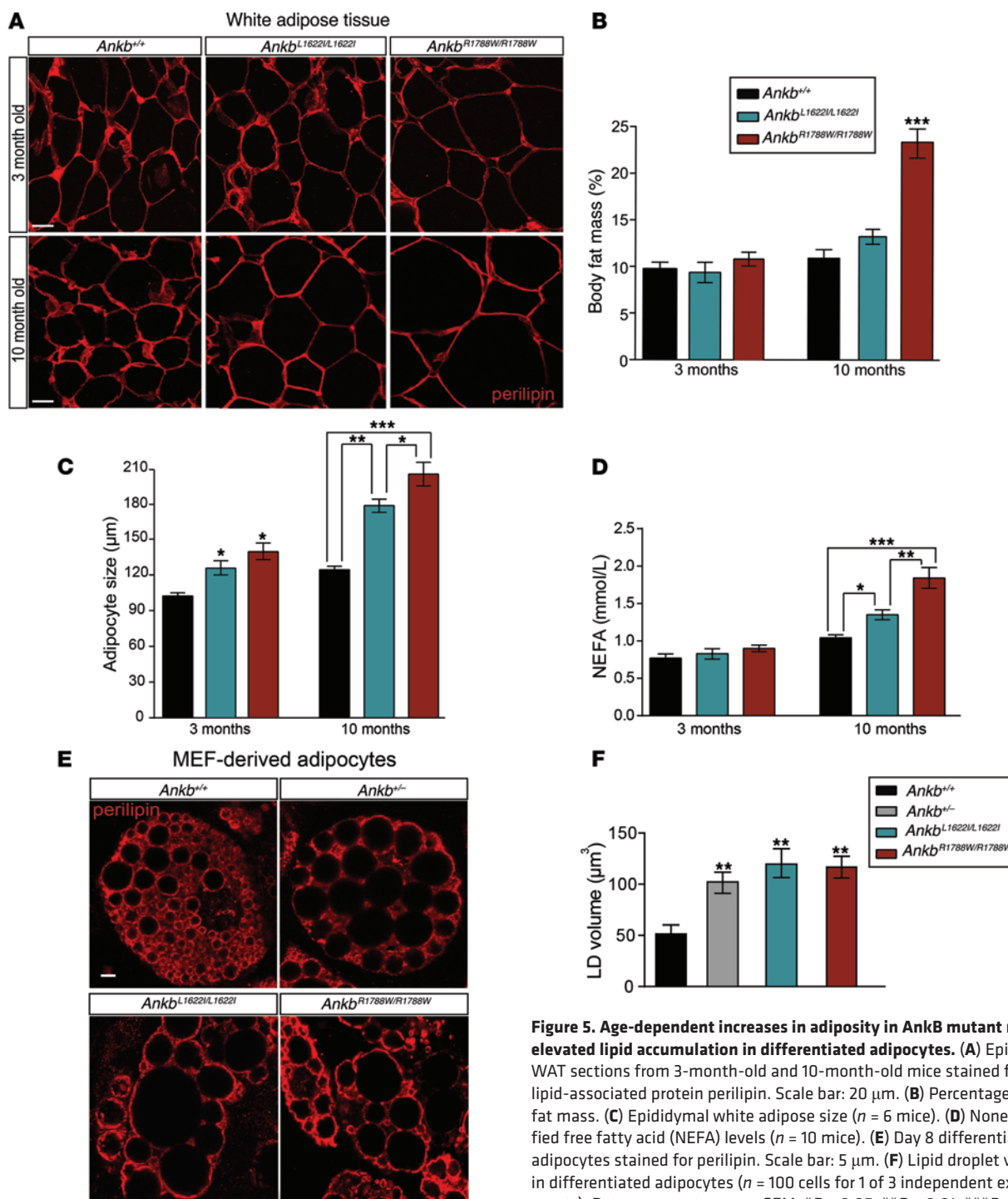


Figure 5. Age-dependent increases in adiposity in *Ank*B mutant mice and elevated lipid accumulation in differentiated adipocytes. (A) Epididymal WAT sections from 3-month-old and 10-month-old mice stained for the lipid-associated protein perilipin. Scale bar: 20 μ m. (B) Percentage of body fat mass. (C) Epididymal white adipocyte size ($n = 6$ mice). (D) Nonesterified free fatty acid (NEFA) levels ($n = 10$ mice). (E) Day 8 differentiated adipocytes stained for perilipin. Scale bar: 5 μ m. (F) Lipid droplet volume in differentiated adipocytes ($n = 100$ cells for 1 of 3 independent experiments). Data represent mean \pm SEM. * $P < 0.05$, ** $P < 0.01$, *** $P < 0.001$, 1-way ANOVA with post-hoc Tukey test.

mental Figure 9). Together, our data indicate that changes in transcriptional activation are likely secondary to the process of adipocyte differentiation in vitro and do not reflect a role for *Ank*B in the transcriptional regulation of adipogenesis genes.

*Ank*b knockin mice are more susceptible to metabolic consequences of a high-fat diet. The increased size of adipocytes in young *Ank*b^{L1622I/L1622I} or *Ank*b^{R1788W/R1788W} mice, despite normal total body weight (Figure 5, A–C), prompted us to assess effects of a high-fat eucaloric diet (HFD). We found that the obesity, insulin resistance,

and hepatic steatosis (based on liver appearance) phenotypes normally induced by the HFD were more severe in both *Ank*b^{R1788W/R1788W} and *Ank*b^{L1622I/L1622I} mice than in control animals, even though the majority of these parameters were similar among young animals on a normal diet across genotypes (Figure 7, A–C, F, and G). HFD-fed homozygous knockin mice also showed higher fasting glucose levels and significant oral glucose intolerance (Figure 7, D and E). It is notable that GLUT4 overexpression in adipocytes did not protect HFD-fed *Ank*b^{L1622I/L1622I} or *Ank*b^{R1788W/R1788W} mice from glucose intolerance (47).

The R1788W AnkB mutation promotes age-dependent insulin resistance. Obesity and hyperlipidemia are associated with the development of insulin resistance and with hyperglycemia in humans and other species. Therefore, using aged *Ankb*^{L1622I/L1622I} or *Ankb*^{R1788W/R1788W} mice maintained on a regular diet, we next evaluated whole-body glucose responses, which demonstrated the characteristic increased adiposity and elevated levels of free fatty acids (Figure 5, A–D). Not surprisingly, 10-month-old *Ankb*^{R1788W/R1788W} mice exhibited elevated fasting glucose levels and impaired oral glucose tolerance (Figure 8, A and B). In addition, hyperinsulinemic-euglycemic clamp measurements revealed that *Ankb*^{R1788W/R1788W} mice had become less responsive to insulin with age (Figure 8C), as evidenced by a reduction in GIR (29%), a significantly lower 2-deoxy-glucose glucose uptake by muscle (21%) and WAT (37%) (Figure 8, D–F), and a marked loss (91%) of the ability of the liver to suppress EGP (Supplemental Figure 5, C and D). Importantly, insulin resistance was accompanied by decreased activation of insulin signaling in both WAT and skeletal muscle (Figure 8, G and H). Thus, our results indicate that age-dependent increases in adiposity combined with primary pancreatic β cell insufficiency trigger the onset of severe metabolic abnormalities in older *Ankb*^{R1788W/R1788W} animals.

Ankb^{R1788W/+} mice have shortened life spans and demonstrate obesity and hyperglycemia with age. Since the L1622I and R1788W AnkB variants are predominantly found in heterozygous carriers in human populations, we assessed the long-term effects of these variants in heterozygous mice. Overall, body weight and fasting glucose levels were increased with age in both control and *Ankb*^{R1788W/+} and *Ankb*^{L1622I/+} knockin mice, but these changes were more pronounced in *Ankb*^{R1788W/+} mice (Supplemental Figure 10, A and B), which also exhibited shorter life spans. In particular, *Ankb*^{R1788W/+} animals had a median survival of 794 days compared with 896 days for *Ankb*^{+/+} mice and 855 days for *Ankb*^{L1622I/+} mice ($P = 0.005$, Supplemental Figure 10, C and D). It is likely that metabolic deficits described here, combined with the more deleterious impact of the R1788W variant on heart function noted in humans (17), contributed to the significantly reduced life span of *Ankb*^{R1788W/+} mice.

Discussion

A major challenge in understanding the recent epidemic in metabolic disorders in modern Western societies is the identification of susceptibility loci that are predominantly expressed under conditions of high-caloric diets and extended life span. We report a previously uncharacterized metabolic syndrome due to an R1788W AnkB mutation shared by nearly one million North Americans, which in mice combines pancreatic β cell dysfunction, characterized by impaired insulin secretion due to InsP3R deficiency, and age-dependent adiposity and insulin resistance, which is associated with increased cell surface GLUT4 and with sustained elevations in glucose uptake in skeletal muscle and fat. In young AnkB knockin mice bearing the T2D-associated R1788W variant, insulin secretion deficits (Figure 2, B and C) were compensated by increased peripheral glucose uptake through persistent cell surface GLUT4 (Figure 3, C, D, G, and I). *Ankb*^{R1788W/R1788W} mice developed metabolic defects, including increased adiposity, elevated fasting glucose, and insulin resistance with age or following a

HFD (Figures 5–8). Extrapolating to humans, the metabolic costs associated with the R1788W AnkB mutation would likely have been blunted in earlier times before modern increases in longevity and caloric intake.

An unexpected finding was that both R1788W and L1622I AnkB mutations resulted in a tissue-specific reduction in AnkB polypeptide levels (Figure 1). Interestingly, *Ankb*^{+/-} haploinsufficient mice also exhibited deficits in oral glucose tolerance and insulin secretion (19) and significant increases in cell surface GLUT4, in glucose uptake in adipocytes, and in lipohypertrophy (Figures 3–5). These findings demonstrate that the pathological effects of these AnkB variants are caused, at least in part, by AnkB haploinsufficiency. However, the more pronounced metabolic phenotypes observed in *Ankb*^{R1788W/R1788W} and *Ankb*^{R1788W/+} mice and in cultured cells suggest additional functional effects of the R1788W variant. Interestingly, the R1788W mutation is located on the surface of a predicted amphipathic α -helix in the AnkB's C-terminal regulatory domain and modulates the affinity of AnkB for binding partners, such as the sarcomere protein obscurin (48) and heat shock protein 40 (Hsp40) (49). In contrast, the molecular consequences of the L1622I mutation are not known. Thus, while R1788W and L1622I AnkB variants are both tissue-specific hypomorphs, the R1788W mutation, in addition, results in altered intrinsic function.

Ankb^{L1622I/L1622I} mice exhibited a milder pancreatic phenotype than R1788W mice but still shared an increased sensitivity to the metabolic consequences of a HFD (Figure 7). These results suggest the possibility that other mutations of AnkB identified as being functionally significant based on their association with cardiac arrhythmia (15–18) may also cause AnkB deficiency and increased susceptibility to pathological consequences of Western diets. These ANKB mutations occur with a cumulative prevalence of about 2% in individuals of mixed European descent and of over 7% in African Americans (ref. 16 and Figure 1A), which together represent a population large enough to contribute to public health.

An unusual feature of AnkB metabolic syndrome due to the R1788W mutation is the combination of early pancreatic β cell insufficiency with increased glucose uptake by peripheral tissues, leading to age-dependent adiposity and insulin resistance. Patients with this condition would likely present as middle-aged adults with features of both type 1 diabetes and T2D. Interestingly, a subset of diabetes referred to as “double diabetes” also presents with initial loss of pancreatic islet function in combination with insulin resistance (50, 51). However, while most of these patients have autoimmune antibodies, those with AnkB metabolic syndrome would probably experience impaired insulin secretion without involving the immune system.

Despite extensive studies on insulin-dependent delivery of GLUT4 transporters to the plasma membrane, mechanisms for internalization of GLUT4 following cessation of insulin signaling are less well established (31, 32, 52). Multiple reports provide evidence for both clathrin-mediated endocytosis-dependent (CME-dependent) and CME-independent mechanisms of GLUT4 internalization in adipocytes and muscle cells. The degree of activation of one pathway versus the other and the type of CME-independent route used depends on the cell type

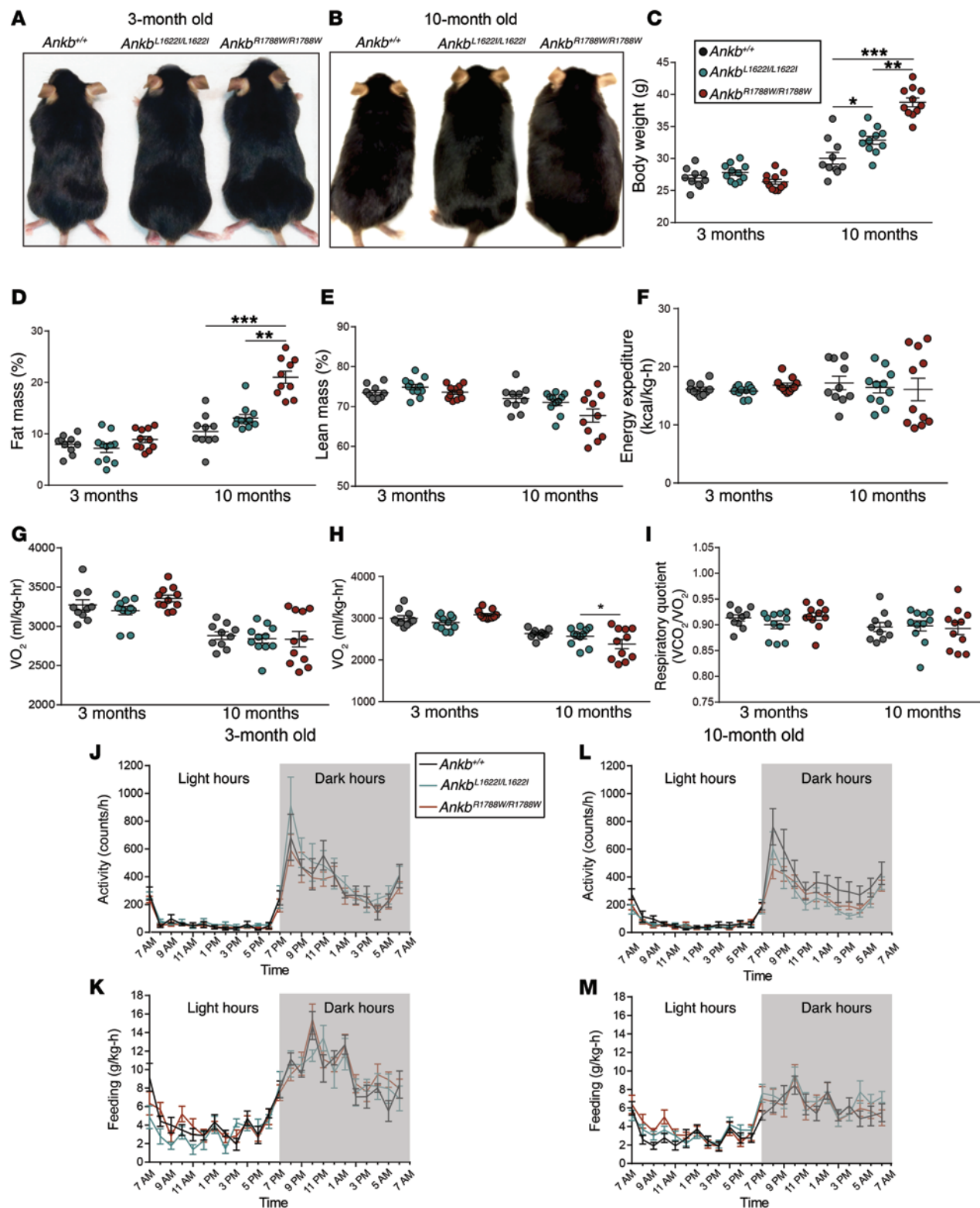


Figure 6. Increased adiposity in *Ankbr*^{R1788W/R1788W} mutant mice is not caused by major changes in appetite or activity. (A and B) Representative images of congenic *Ankbr*^{+/+}, *Ankbr*^{L1622I/L1622I}, and *Ankbr*^{R1788W/R1788W} (A) 3-month-old and (B) 10-month-old male mice. (C) Body weight. (D) Fat mass and (E) lean mass as a percentage of body weight. (F) Average 24-hour energy expenditure, (G) oxygen consumption, (H) CO₂ production measured by CLAMS. (I) Respiratory quotient. (J and L) Activity during a 24-hour period for (J) 3-month-old and (L) 10-month-old mice. (K and M) Food consumption on a regular diet during a 24-hour period for (K) 3-month-old and (M) 10-month-old mice. Data represent mean ± SEM, (*n* = 8, 3-month-old mice and *n* = 10, 10-month-old mice) for 1 experiment. **P* < 0.05, ***P* < 0.01, ****P* < 0.001, 1-way ANOVA with post-hoc Tukey test.

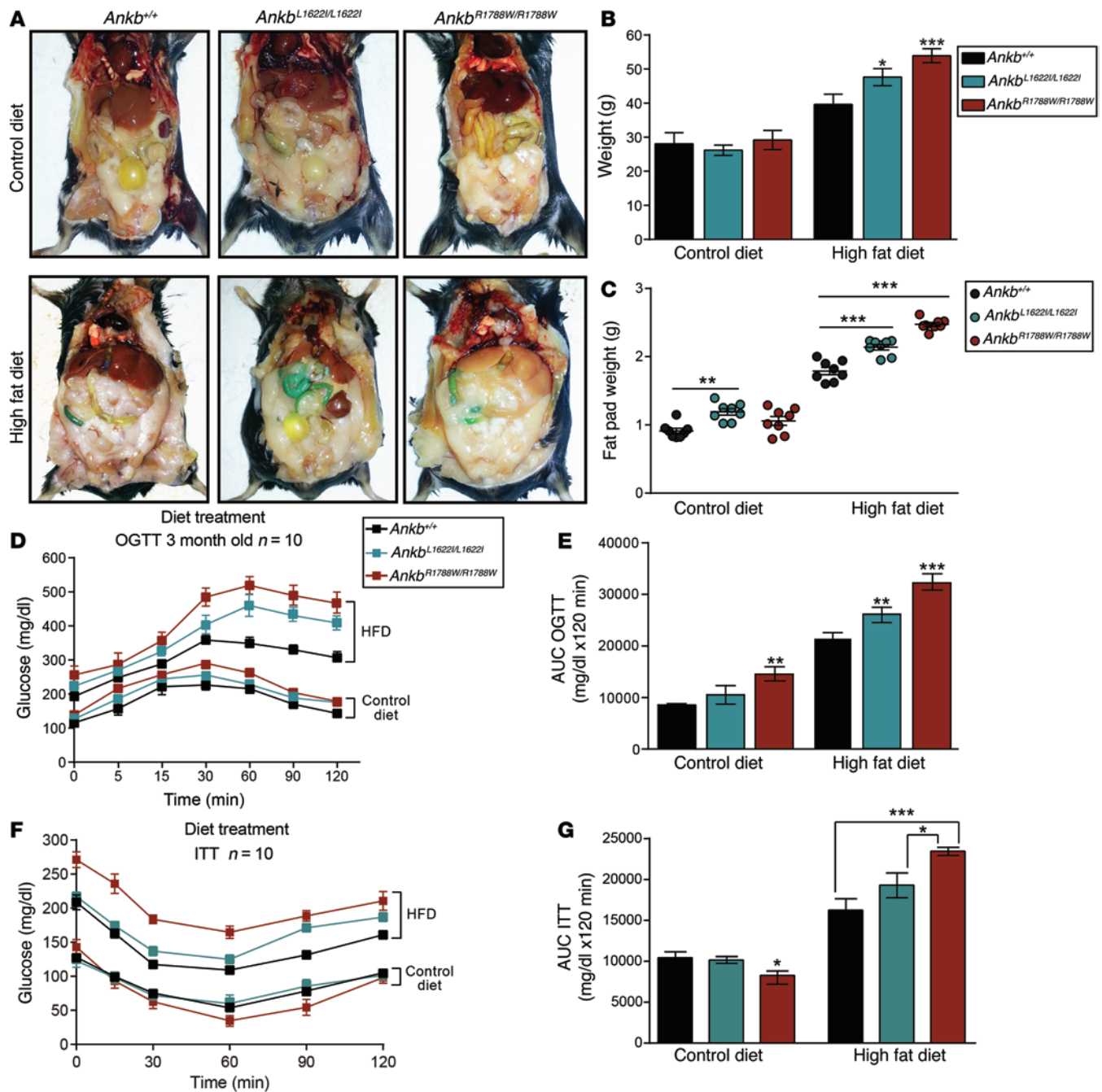


Figure 7. Ankb knockin mice are more susceptible to HFD-induced metabolic derangements and obesity. (A) Representative images of 3-month-old *Ankb*^{+/+}, *Ankb*^{L1622I/L1622I}, and *Ankb*^{R1788W/R1788W} mice fed either a control or a HFD for 12 weeks. (B) Body weight. (C) Epididymal fat-pad weights. (D) Blood glucose levels in response to oral glucose (2 mg/kg body weight) during an OGTT. (E) Area under the curve for OGTT. (F) Blood glucose levels in response to insulin administration (0.75 U/kg body weight). (G) Area under the curve for the intraperitoneal insulin tolerance test (ITT). Data represent mean ± SEM (n = 12 mice per group for 1 experiment). *P < 0.05, **P < 0.01, ***P < 0.001, 1-way ANOVA with post-hoc Tukey test.

and, importantly, on the insulin stimulation stage of the cell (52–59). In addition, several studies suggest that the interaction between the μ 2-adaptin subunit of the clathrin adaptor AP-2 and the phenylalanine (F⁵) residue within the GLUT4 N-terminal F⁵QQI⁸ motif is the predominant signal that sorts GLUT4 to clathrin-coated pits (60, 61). However, adaptors other than AP-2 may mediate GLUT4 association with the endocytic machinery since silencing of AP-2 in adipocytes reduced GLUT4 internal-

ization only in insulin-stimulated cells, even though GLUT4 colocalizes with clathrin puncta and is still internalized through CME in the basal state (37, 54).

The following findings suggest that AnkB functions as a heretofore undescribed adaptor that either by direct interaction with the GLUT4 transporter or through other proteins promotes GLUT4 retrieval from the cell surface. First, AnkB coimmunoprecipitated with GLUT4 from skeletal muscle lysates and

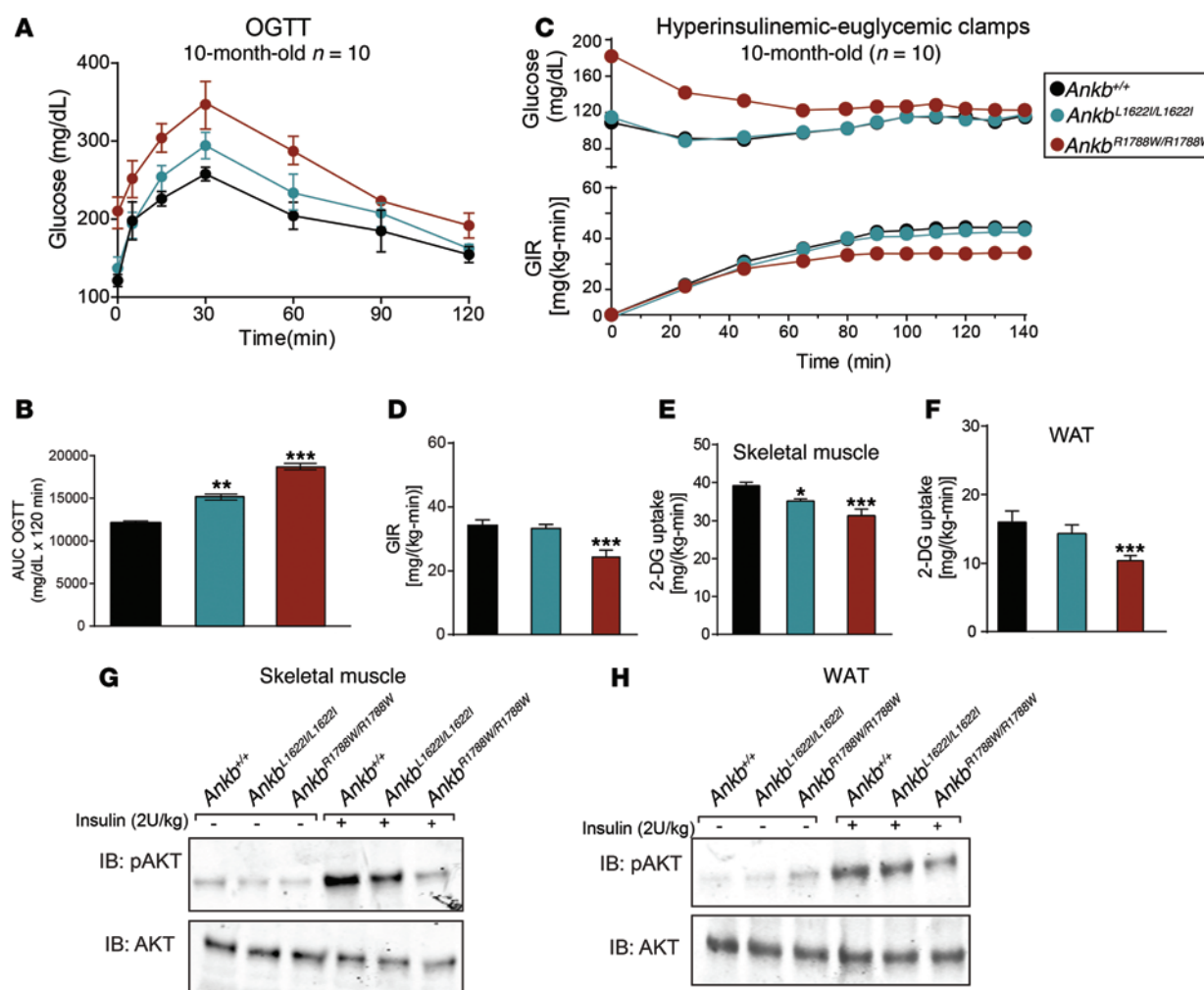


Figure 8. Age-dependent changes in glucose levels and insulin sensitivity in *AnkB*^{R1788W/R1788W} mice. (A) Blood glucose levels in response to oral glucose (2 mg/kg body weight). (B) Area under the curve for the OGTT. (C) Hyperinsulinemic-euglycemic clamp analysis in 10-month-old mice ($n = 10$). (D) GIR during insulin clamp. (E and F) 2-DG uptake by (E) skeletal muscle and (F) WAT. (G and H) Immunoblots of total AKT and phosphorylated AKT (p-AKT S473) levels in (G) skeletal muscle and (H) WAT from 10-month-old mice ($n = 6$ mice) under basal or insulin-stimulated conditions. Data from G and H are representative of 3 independent experiments. All data represent mean \pm SEM. * $P < 0.05$, ** $P < 0.01$, *** $P < 0.001$, 1-way ANOVA with post-hoc Tukey test.

when these proteins were coexpressed in HEK293 cells (Figure 4, B and F). Second, reduction of AnkB levels, either by protein knockdown (data not shown) or by expression of the human variants, resulted in both slower GLUT4 internalization rates and in persistent plasma membrane association of GLUT4 in skeletal muscle and adipocytes (Figure 3, G and I, and Figure 4, D and E). Third, AnkB regulates intracellular organelle transport through dual interactions with PtdIns3(P)-enriched endocytic membranes and with the dynein/dynactin retrograde motor complex (12–14), both of which have demonstrated roles in GLUT4 trafficking (62, 63). Fourth, AnkB directly binds several members of the EHD/RME family of endosome-based scaffolding molecules suggested to mediate different steps of GLUT4 intracellular traffic (33–35). Fifth, the N-terminal domain of clathrin heavy chain binds with high affinity to the membrane-binding domain of ankyrin, and this interaction is required for budding of clathrin-coated pits from the membrane and for the internalization of the low-density lipoprotein receptor (36). Last, AnkB

required the F⁵QQI⁸ motif of GLUT4 for coimmunoprecipitation (Figure 4F). Moreover, the internalization-deficient F5A Myc-GLUT4-GFP mutant was resistant to the effects of AnkB deficiency in R1788W adipocytes (Figure 4, C–E), suggesting that AnkB regulates GLUT4 internalization through a mechanism that requires the interaction of the GLUT4 FQQI motif with the endocytic machinery.

R1788W *AnkB* knockin mice developed age-dependent increases in adiposity without marked changes in food consumption or activity. Interestingly, *AnkB*^{R1788W/R1788W} as well as *AnkB*^{L1622I/L1622I} differentiated adipocytes showed cell-autonomous increases in adipocyte number and enlarged lipid droplets. Our observations suggest a mechanism for age-dependent adiposity that is independent of major changes in appetite or activity and is rather caused by elevation in cell surface-associated GLUT4. It is likely that persistent glucose influx, which supplies adipocytes with lipid synthesis precursors, contributes to increased adipocyte number and size.

A major challenge in the management of T2D is the phenotypic heterogeneity of the disease, which results in differences in patient responses to treatments. Identifying and characterizing distinct subcategories of T2D with unique biology, like the one described in this study, may facilitate early disease prognosis and guide the choice of treatment. In this case, patients with *ANKB* mutations could become prime candidates for early intervention through personalized therapies. Based on our results in knockin mice, we predict that, in the case of R1788W carriers, in addition to following a healthy lifestyle, it would be beneficial for them to manage their metabolic syndrome at early stages, using a combination strategy that promotes noncholinergic stimulation of insulin secretion by agents such as incretins (64) as well as agents such as α -glucosidase inhibitors and diets that reduce hyperglycemia.

In summary, we identify a metabolic syndrome due to the human *AnkB* R1788W variants present in 0.3% of individuals of mixed European descent that combines early-onset abnormal pancreatic β cell function with age- and diet-dependent increased adiposity. Intriguingly, additional *AnkB* variants, some of which are known to directly affect cardiac function (15–18), might also affect glucose homeostasis and related disorders with distinct presentations in different ethnic populations. In particular, the L1622I allele shown in this study to increase susceptibility to a HFD is shared by 7% of African Americans, or about the same prevalence as the trait for sickle cell anemia, and would be predicted to be present in homozygotes at a frequency of about 0.1%. Given the differences between mice and humans, it will be critical to evaluate metabolic effects of *ANKB* variation in human subjects, including those homozygous for the L1622I mutation.

Methods

Mouse lines and animal care. All studies were conducted in 3-month-old or 10-month-old congenic male mice. *Ankb*^{-/-} mice have been previously described (18). *Itrp1*^{-/-} mice were purchased from The Jackson Laboratory (stock 000019). *Ankb* knockin mice bearing either the p.L1622I or p.R1788W human variants were generated with help from the Duke Transgenic Mouse Facility (see Supplemental Methods). All mice were housed at 22°C \pm 2°C on a 12-hour-light/12-hour-dark cycle and fed ad libitum regular chow and water. For HFD studies, 4-week-old male mice were divided into 2 groups of 12 mice each and fed ad libitum either control diet or HFD for a total period of 12 weeks. On a caloric basis, the control diet consisted of 10% fat, 20% protein, and 70% carbohydrate (Purina TestDiet 58Y2). For the HFD, 60% of the calories were in the form of fat, 20% of the calories were from protein, and 20% of the calories were from carbohydrates (Purina TestDiet 58V8).

Tolerance tests and measurement of plasma metabolites. Mice were fasted for 14 hours, and blood glucose was measured by tail bleeding at 0, 15, 30, 60, 90, and 120 minutes after glucose administration by oral gavage. For insulin tolerance tests, mice were administered 0.75 U/kg body weight of recombinant human insulin (Humulin R, Elli Lilly) by intraperitoneal injection.

Metabolic cage analysis and hyperinsulinemic-euglycemic clamp study. Metabolic cage analysis and clamp studies were conducted at the Yale Mouse Metabolic Phenotyping Center (MMPC) following recommendations of the MMPC Consortium (65). Body composition was determined by ¹H magnetic resonance spectroscopy

(Bruker Minispec). The comprehensive lab animal monitoring system (CLAMS, Columbus Instruments) was used to evaluate activity, energy expenditure, feeding, drinking, and respiratory quotient over the course of 48 hours. The data presented in graphs are the 24-hour averages normalized to body weight. Clamps were performed following a previously described protocol (66).

MEF cultures and differentiation into adipocytes. Primary MEF cultures were established from postnatal day 0 mice. 48 hours after confluence, MEFs were induced to undergo adipogenic differentiation.

Gene expression analysis. Total RNA was isolated from cells or tissues using the RNeasy Kit or the RNeasy Lipid Tissue Kit (Qiagen) and DNase treatment. Quantitative PCR was performed with the Applied Biosystems 7500 Fast RT-PCR system and SYBR Green detection reagent using cDNA synthesized with the SuperScript III First-Strand Synthesis System (Invitrogen). Primer sequences are provided in the Supplemental Methods. Gene expression analysis of adipocyte genes was conducted at the Duke Microarray Shared Resource (Duke University). 500 ng of total RNA was amplified according to the MessageAmp Premier protocol (Ambion) and hybridized to the Mouse 430 2.0 GeneChip (Affymetrix) according to the manufacturer's instructions. Partek Genomics Suite 6.6 (Partek Inc.) was used to perform data analysis.

Membrane fractionation assay. 3-month-old male mice were fasted overnight and injected subcutaneously either 0.5 U/kg insulin or saline solution. Hind limb muscles and epididymal fat pads were carefully dissected out 30 minutes after injection and snap-frozen in liquid nitrogen. Plasma membrane fractions from skeletal muscle or adipose tissue lysates were obtained by differential ultracentrifugation as described previously (67, 68). We also used a similar protocol for isolation of plasma membrane fractions from differentiated adipocytes (68).

2-Deoxy-D-glucose uptake assay. Differentiated adipocytes cultured in 12-well plates were assessed for their ability to uptake glucose 9 days after induction of differentiation following a previously published protocol (69).

Quantification of insulin signaling pathway. Changes in the activation of the insulin pathway were assessed from total protein lysates from differentiated adipocytes that were either untreated (time 0) or stimulated with 100 nM insulin. For in vivo analysis, mice were fasted for 8 hours and administered either saline solution (untreated) or 0.8 U/kg insulin through intraperitoneal injection. Cells were collected at various time points after treatment with insulin, and tissues were collected 20 minutes after treatment. Immunoblotting of total lysates was performed using anti-AKT and anti-p-AKT (S473) antibodies.

Analysis of GLUT4 translocation and endocytosis by immunofluorescence. Differentiated adipocytes expressing Myc-GLUT4-GFP alone or in combination with 3xHA-*AnkB* were starved in serum-free DMEM containing 0.2% BSA for 2 hours at 37°C. Cells were either treated or not (basal) with 100 nM insulin for 30 minutes at 37°C. The population of plasma membrane-associated GLUT4 was labeled with mouse anti-Myc antibody for 1 hour on ice. Cells were then either fixed with 4% PFA (basal and time 0) or incubated at 37°C for 5, 10, 15, 20, and 30 minutes to allow for GLUT4 internalization.

Image acquisition. Fluorescent antibody and dye labeling was visualized using a 780 laser scanning confocal microscope (Zeiss). Z-stacks with optical sections of 0.5- μ m intervals were collected using the \times 20 (0.8 NA) and \times 40 oil (1.3 NA) objective lens. Single plain images of Oil Red O-stained adipocytes were taken using the \times 20 objective lens of a TE200 inverted microscope (Nikon).

Statistics. GraphPad Prism (GraphPad Software) was used for statistical analysis. Two groups of measurements were compared by unpaired, 2-tailed Student's *t* test. Multiple groups were compared by repeated-measures 1-way ANOVA, followed by a post-hoc Tukey test. Survival curves were compared by a Mantel-Cox test. Results are presented as mean \pm SEM. $P \leq 0.05$ was considered significant.

Study approval. Experimental procedures were approved by the Institutional Animal Care and Use Committee of Duke University.

Acknowledgments

We thank J.S. Bogan for the gift of the Myc7x-GLUT4-GFP construct, Gerald I. Shulman and Michael Jurczak at the Yale MMPC for technical assistance with the studies, the Duke Transgenic

Mouse Facility for help generating the knockin mice, the Duke Microarray Shared Resource facility for help with gene expression analysis, and Christopher B. Newgard, Deborah Muoio, and Larry Moss at the Duke Molecular Physiology Institute for their valuable suggestions. M. Zhang acknowledges grant support (663812 and AoE/M09/12) from the Research Grant Council of Hong Kong. Mouse metabolic cage and insulin clamp analysis were supported by Yale MMPC grant U24 DK-059635.

Address correspondence to: Vann Bennett, Duke University Medical Center, 214A Nanaline Duke, 307 Research Drive, Box 3711, Durham, North Carolina 27710, USA. Phone: 919.684.3538; E-mail: vann.bennett@dm.duke.edu.

- World Health Organization. World Health Organization Obesity Fact Sheet No. 311. WHO Web site. <http://www.who.int/mediacentre/factsheets/fs311/en/>. Updated January 2015. Accessed June 3, 2015.
- World Health Organization. World Health Organization Obesity Fact Sheet No. 312. WHO Web site. <http://www.who.int/mediacentre/factsheets/fs312/en/>. Updated January 2015. Accessed June 3, 2015.
- Drong AW, Lindgren CM, McCarthy MI. The genetic and epigenetic basis of type 2 diabetes and obesity. *Clin Pharmacol Ther*. 2010;92(6):707-715.
- Lyssenko V, et al. Common variant in MTNR1B associated with increased risk of type 2 diabetes and impaired early insulin secretion. *Nat Genet*. 2009;41(1):82-88.
- Rung J, et al. Genetic variant near IRS1 is associated with type 2 diabetes, insulin resistance and hyperinsulinemia. *Nat Genet*. 2009;41(10):1110-1115.
- Manolio TA, et al. Finding the missing heritability of complex diseases. *Nature*. 2009;461(7265):747-753.
- Pal A, McCarthy MI. The genetics of type 2 diabetes and its clinical relevance. *Clin Genet*. 2013;83(4):297-306.
- Rosenberg NA, Huang L, Jewett EM, Szpiech ZA, Jankovic I, Boehnke M. Genome-wide association studies in diverse populations. *Nat Rev Genet*. 2010;11(5):356-366.
- Tennessen JA, et al. Evolution and functional impact of rare coding variation from deep sequencing of human exomes. *Science*. 2012;337(6090):64-69.
- Grarup N, Sandholt CH, Hansen T, Pedersen O. Genetic susceptibility to type 2 diabetes and obesity: from genome-wide association studies to rare variants and beyond. *Diabetologia*. 2014;57(8):1528-1541.
- Bennett V, Lorenzo DN. Spectrin- and ankyrin-based membrane domains and the evolution of vertebrates. *Curr Top Membr*. 2013;72:1-37.
- Ayalon G, Davis JQ, Scotland PB, Bennett V. An ankyrin-based mechanism for functional organization of dystrophin and dystroglycan. *Cell*. 2008;135(7):1189-1200.
- Ayalon G, Hostettler JD, Hoffman J, Kizhatil K, Davis JQ, Bennett V. Ankyrin-B interactions with spectrin and dynactin-4 are required for dystrophin-based protection of skeletal muscle from exercise injury. *J Biol Chem*. 2011;286(9):7370-7378.
- Lorenzo DN, et al. A PIK3C3-Ankyrin-B-Dynactin pathway promotes axonal growth and multiorganelle transport. *J Cell Biol*. 2014;207(6):735-752.
- Mohler PJ, et al. Ankyrin-B mutation causes type 4 long-QT cardiac arrhythmia and sudden cardiac death. *Nature*. 2003;421(6923):634-639.
- Mohler PJ, et al. A cardiac arrhythmia syndrome caused by loss of ankyrin-B function. *Proc Natl Acad Sci U S A*. 2004;101(24):9137-9142.
- Mohler PJ, et al. Defining the cellular phenotype of "ankyrin-B syndrome" variants: human ANK2 variants associated with clinical phenotypes display a spectrum of activities in cardiomyocytes. *Circulation*. 2007;115(4):432-441.
- Mohler PJ, et al. Ankyrin-B syndrome: enhanced cardiac function balanced by risk of cardiac death and premature senescence. *PLoS One*. 2007;2(10):e1051.
- Healy JA, et al. Cholinergic augmentation of insulin release requires ankyrin-B. *Sci Signal*. 2010;3(113):ra19.
- Exome Variant Server, NHLBI GO Exome Sequencing Project (ESP). University of Washington Web site. <http://evs.gs.washington.edu/EVS>. Accessed June 3, 2015.
- 1000 Genomes Project Consortium, et al. An integrated map of genetic variation from 1,092 human genomes. *Nature*. 2012;491(7422):56-65.
- Wang C, Yu C, Ye F, Wei Z, Zhang M. Structure of the ZU5-ZU5-UPA-DD tandem of ankyrin-B reveals interaction surfaces necessary for ankyrin function. *Proc Natl Acad Sci U S A*. 2012;109(13):4822-4827.
- Nilsson T, Arkhammar P, Hallberg A, Hellman B, Berggren PO. Characterization of the inositol 1, 4, 5-trisphosphate-induced Ca²⁺ release in pancreatic β -cells. *Biochem J*. 1987;248(2):329-336.
- Dyachok O, Tufveson G, Gylfe E. Ca²⁺-induced Ca²⁺ release by activation of inositol 1,4,5-trisphosphate receptors in primary pancreatic β -cells. *Cell Calcium*. 2004;36(1):1-9.
- Ye R, et al. Inositol 1, 4, 5-trisphosphate receptor 1 mutation perturbs glucose homeostasis and enhances susceptibility to diet-induced diabetes. *J Endocrinol*. 2011;210(2):209-217.
- James DE, Brown R, Navarro J, Pilch PF. Insulin-regulatable tissues express a unique insulin-sensitive glucose transport protein. *Nature*. 1998;333(6169):183-185.
- Larance M, Ramm G, James DE. The GLUT4 code. *Mol Endocrinol*. 2008;22(2):226-233.
- Cho H, et al. Insulin resistance and a diabetes mellitus-like syndrome in mice lacking the protein kinase Akt2 (PKB β). *Science*. 2001;292(5522):1728-1731.
- Ng Y, Ramm G, Lopez JA, James DE. Rapid activation of Akt2 is sufficient to stimulate GLUT4 translocation in 3T3-L1 adipocytes. *Cell Metab*. 2008;7(4):348-356.
- Lizunov VA, et al. Insulin stimulates fusion, but not tethering, of GLUT4 vesicles in skeletal muscle of HA-GLUT4-GFP transgenic mice. *Am J Physiol Endocrinol Metab*. 2012;302(8):E950-E960.
- Foley K, Boguslavsky S, Klip A. Endocytosis, recycling, and regulated exocytosis of glucose transporter 4. *Biochemistry*. 2011;50(15):3048-3061.
- Hou JC, Pessin JE. Ins (endocytosis) and outs (exocytosis) of GLUT4 trafficking. *Curr Opin Cell Biol*. 2007;19(4):466-473.
- Gudmundsson H, et al. EH domain proteins regulate cardiac membrane protein targeting. *Circ Res*. 2010;107(1):84-95.
- Guilherme A, et al. EHD2 and the novel EH domain binding, EHBP1 couple endocytosis to the actin cytoskeleton. *J Biol Chem*. 2004;279(11):10593-10605.
- Guilherme A, Soriano NA, Fucini PS, Czech MP. Role of EHD1 and EHBP1 in perinuclear sorting and insulin-regulated GLUT4 recycling in 3T3-L1 adipocytes. *J Biol Chem*. 2004;279(38):40062-40075.
- Michaely P, Kamal A, Anderson RG, Bennett V. A requirement for ankyrin binding to clathrin during coated pit budding. *J Biol Chem*. 1999;274(50):35908-35913.
- Huang S, et al. Insulin stimulates membrane fusion and GLUT4 accumulation in clathrin coats on adipocyte plasma membranes. *Mol Cell Biol*. 2007;27(9):3456-3469.
- Garippa RJ, Judge TW, James DE, McGraw TE. The amino terminus of GLUT4 functions as an internalization motif but not an intracellular retention signal when substituted for the transferrin receptor cytoplasmic domain. *J Cell Biol*.

- 1994;124(5):705–715.
39. Piper RC, et al. The efficient intracellular sequestration of the insulin-regulatable glucose transporter (GLUT-4) is conferred by the NH2 terminus. *J Cell Biol.* 1992;117(4):729–743.
 40. Piper RC, et al. GLUT-4 NH2 terminus contains a phenylalanine-based targeting motif that regulates intracellular sequestration. *J Cell Biol.* 1993;121(6):1221–1232.
 41. Wang C, et al. Structural basis of diverse membrane target recognitions by ankyrins. *Elife.* 2014;3.
 42. Shepherd PR, Gnudi L, Tozzo E, Yang H, Leach F, Kahn BB. Adipose cell hyperplasia and enhanced glucose disposal in transgenic mice overexpressing GLUT4 selectively in adipose tissue. *J Biol Chem.* 1993;268(30):22243–22246.
 43. Tozzo E, Shepherd PR, Gnudi L, Kahn BB. Transgenic GLUT-4 overexpression in fat enhances glucose metabolism: preferential effect on fatty acid synthesis. *Am J Physiol.* 1995;268(5 pt 1):E956–E964.
 44. Pedersen O, Kahn CR, Kahn BB. Divergent regulation of the Glut 1 and Glut 4 glucose transporters in isolated adipocytes from Zucker rats. *J Clin Invest.* 1992;89(6):1964–1973.
 45. Lee EB, Ahima RS. Alteration of hypothalamic cellular dynamics in obesity. *J Clin Invest.* 2012;122(1):22–25.
 46. Thaler JP, et al. Obesity is associated with hypothalamic injury in rodents and humans. *J Clin Invest.* 2012;122(1):153–162.
 47. Gnudi L, Tozzo E, Shepherd PR, Bliss JL, Kahn BB. High level overexpression of glucose transporter-4 driven by an adipose-specific promoter is maintained in transgenic mice on a high fat diet, but does not prevent impaired glucose tolerance. *Endocrinology.* 1995;136(3):995–1002.
 48. Cunha SR, Mohler PJ. Obscurin targets ankyrin-B and protein phosphatase 2A to the cardiac M-line. *J Biol Chem.* 2008;283(46):31968–31980.
 49. Mohler PJ, et al. Isoform specificity among ankyrins. An amphipathic alpha-helix in the divergent regulatory domain of ankyrin-b interacts with the molecular co-chaperone Hdj1/Hsp40. *J Biol Chem.* 2004;279(24):25798–25804.
 50. Cleland SJ, Fisher BM, Colhoun HM, Sattar N, Petrie JR. Insulin resistance in type 1 diabetes: what is ‘double diabetes’ and what are the risks? *Diabetologia.* 2013;56(7):1462–1470.
 51. Teupe B, Bergis K. Epidemiological evidence for “double diabetes”. *Lancet.* 1991;337(8737):361–362.
 52. Antonescu CN, Foti M, Sauvonnet N, Klip A. Ready, set, internalize: mechanisms and regulation of GLUT4 endocytosis. *Biosci Rep.* 2009;29(1):1–11.
 53. Li Q, et al. Ca²⁺ signals promote GLUT4 exocytosis and reduce its endocytosis in muscle cells. *Am J Physiol Endocrinol Metab.* 2014;307(2):E209–E224.
 54. Antonescu CN, Diaz M, Femia G, Planas JV, Klip A. Clathrin-dependent and independent endocytosis of glucose transporter 4 (GLUT4) in myoblasts: regulation by mitochondrial uncoupling. *Traffic.* 2008;9(7):1173–90.
 55. Wijesekera N, Tung A, Thong FS, Klip A. Muscle cell depolarization induces a gain in surface GLUT4 via reduced endocytosis, independently of AMPK. *Am J Physiol Endocrinol Metab.* 2006;290(6):E1276–E1286.
 56. Blot V, McGraw TE. GLUT4 is internalized by a cholesterol-dependent nystatin-sensitive mechanism inhibited by insulin. *EMBO J.* 2006;25(24):5648–5658.
 57. Ros-Baro A, et al. Lipid rafts are required for GLUT4 internalization in adipose cells. *Proc Natl Acad Sci USA.* 2001;98(21):12050–12055.
 58. Reed SE, et al. A role for Rab14 in the endocytic trafficking of GLUT4 in 3T3-L1 adipocytes. *J Cell Sci.* 2013;126(pt 9):1931–1941.
 59. Hartig SM, et al. The F-BAR protein CIP4 promotes GLUT4 endocytosis through bidirectional interactions with N-WASP and Dynamin-2. *J Cell Sci.* 2009;122(pt 13):2283–2291.
 60. Al-Hasani H, et al. Roles of the N- and C-termini of GLUT4 in endocytosis. *J Cell Sci.* 2002;115(pt 1):131–140.
 61. Bernhardt U, Carlotti F, Hoeber RC, Joost HG, Al-Hasani H. A dual role of the N-terminal FQQ motif in GLUT4 trafficking. *Biol Chem.* 2009;390(9):883–892.
 62. Huang J, Imamura T, Olefsky JM. Insulin can regulate GLUT4 internalization by signaling to Rab5 and the motor protein dynein. *Proc Natl Acad Sci USA.* 2001;98(23):13084–13089.
 63. Lodhi IJ, et al. Insulin stimulates phosphatidylinositol 3-phosphate production via the activation of Rab5. *Mol Biol Cell.* 2008;19(7):2718–2728.
 64. Koliaki C, Doupis J. Incretin-based therapy: a powerful and promising weapon in the treatment of type 2 diabetes mellitus. *Diabetes Ther.* 2011;2(2):101–121.
 65. Ayala JE, et al. NIH Mouse Metabolic Phenotyping Center Consortium. Standard operating procedures for describing and performing metabolic tests of glucose homeostasis in mice. *Dis Model Mech.* 2010;3(9–10):525–534.
 66. Jurczak MJ, et al. Dissociation of inositol-requiring enzyme (IRE1 α)-mediated c-Jun N-terminal kinase activation from hepatic insulin resistance in conditional X-box-binding protein-1 (XBPI) knock-out mice. *J Biol Chem.* 2012;287(4):2558–2567.
 67. Klip A, Ramlal T, Young DA, Holloszy JO. Insulin-induced translocation of glucose transporters in rat hindlimb muscles. *FEBS Lett.* 1987;224(1):224–230.
 68. Miura T, et al. Impairment of insulin-stimulated GLUT4 translocation in skeletal muscle and adipose tissue in the Tsumura Suzuki obese diabetic mouse: a new genetic animal model of type 2 diabetes. *Eur J Endocrinol.* 2001;145(6):785–790.
 69. Kanda H, et al. Adipocytes from Munc18c-null mice show increased sensitivity to insulin-stimulated GLUT4 externalization. *J Clin Invest.* 2005;115(2):291–301.